Matching Virtual Histology RF and IVUS Images for Cardiac Synchronization

Murielle Hadad[1], Monica M S Matsumoto, Sergio Shiguemi Furuie

[1]University of São Paulo, São Paulo, Brazil

Abstract

Intravascular Ultrasound (IVUS) provides detailed measurements of the arterial wall. However, during its acquisition, the contraction of the cardiac muscle provokes a relative motion of the transducer with respect to the artery. Consequently, the acquired images are disordered in space. Therefore, to enhance visualization of the coronary artery, volumes of IVUS images of each cardiac phase are needed, mainly for IVUS images that do not contain any external indicator of phase.

Our solution is to use Virtual histology RF images as references, since they are acquired simultaneously with IVUS images and are synchronized with the ECG signal. Thus, this work presents a synchronization of IVUS images with RF images. The RF/IVUS comparison is based on the correlation within a circular region of interest, which can be automatically optimized by the algorithm. Our results show very good error rates inferior to 3%, though IVUS and RF images have different characteristics.

1.   Introduction

Cardiovascular disease is the most common cause of death in the world [1]. Vital to myocardial irrigation, vessels that develop atherosclerotic disease might increase risk of ischemia, infarction and death. Images of diseased vessels can be acquired from the inside, using Intravascular Ultrasound (IVUS), a catheter based system that provides detailed and accurate measurements of the structures of the arterial wall: lumen and vessel size, plaque area and volume, and the location of key anatomical landmarks. The IVUS catheter is inserted into the artery to be studied and placed in its distal portion [3]. The examination begins when the catheter is withdrawn at a constant speed of 0.5mm/s by an external motor and the transducer captures cross sections of coronary [4]. During the acquisition of IVUS images, the cycle of the contraction of the cardiac muscle happens in cycles, alternating phases of systole and diastole, with variation of blood flow and pressure –hence a relative motion of the transducer with respect to the

artery. The direct consequence is an artefact of "saw-tooth", noticeable in longitudinal view [2].

The work proposed here compensates for the lack of existing methods to correct this effect and therefore enhance the visualization and spatial analysis of the coronary artery. Our method arouse from the fact that Virtual histology RF images are acquired simultaneously with IVUS images. Yet, while IVUS images do not contain any external indicator of phase, RF images are synchronized with the ECG signal and consequently can be used as references. Therefore, by synchronizing IVUS with RF images, we synchronize IVUS with ECG and create the basis to later reconstruct volumes of IVUS images of each cardiac phase and allow further investigations of the rich temporal and spatial content of IVUS images [5].

2.   Material and method

The data used are forty IVUS examinations of a database of the Heart Institute (InCor), Hospital das Clinicas, University of Sao Paulo. IVUS and RF (Fig. 1) images were acquired using Intravascular Ultrasound with Virtual Histology (VH® IVUS) equipment from Volcano Therapeutics. The examinations were from 378 to 1800 images long for IVUS images and from 43 to 217 for RF images. The number of RF images is related to the subject's cardiac rhythm. The pullback speed was 0.5mm/s and the frequency was 20MHz.

To match the pairs of RF and IVUS image, we use the 2D correlation (Matlab, corr2), associating each image or sub-sampled-image of radiofrequency with the corresponding image of IVUS. However, the IVUS image size is 384 * 384 pixels while the RF is 400 * 400 pixels. In addition, the IVUS represents only the envelope of the signal while the RF contains the entire signal. Hence, IVUS look blurred and light whereas RF looks sharp and dark, which can mislead the correlation. Finally, the use of a correlation that would consider the whole frame would not give satisfactory results because it would not be sensitive enough to parts of the image that contain the most important variations of shade and rotational motion. In fact, it would be much enhanced by useless parts of the image (black background for instance) and much diminished by the artifact of the

catheter in the center of the image of RF. Therefore, our main goal is to get a correlation as sensitive as possible, rejecting all the parts of the image that can mislead the two-dimensional correlation that is given by:

$$r = \frac{\sum_m \sum_n (A_{mn} - \bar{A})(B_{mn} - \bar{B})}{\sqrt{(\sum_m \sum_n (A_{mn} - \bar{A})^2)(\sum_m \sum_n (B_{mn} - \bar{B})^2)}} \quad (1)$$

where A_{mn} and B_{mn} are the pixel intensity values of RF and IVUS, mn are the position of the pixel, $\bar{A}$ and $\bar{B}$ are their corresponding averages in a region of interest (ROI). It clearly appears that the higher the number of pixels, the less sensitive the correlation is, as it induces division by a larger sum.

As the images have to be of equal size to use the formula of the correlation, the IVUS images are resized using bi-cubic interpolation, so that they have the same size as the RF images (400*400). We also considered the logarithm of the radio frequency intensity value instead of the original RF values (Fig. 2). Indeed, various publications, such as [6], use band pass filtering techniques, recovery envelope, standardization, and logarithmic compression to obtain images of IVUS (signal envelope) from the RF signal.

In order to compare IVUS and RF images and due to the circular nature of the images, we chose ROIs with a ring shape. We have tried several combinations of ring size by varying the parameters "div" (how many rings divide the image, the center of every ring being the center of the image) and "k" (which ring is chosen as the ROI, where 1 is the most external ring) to be selected at the beginning of the algorithm. The location and thickness of each circular region depend on the values of the parameters k and div. The higher the number of divisions, the smaller the thickness of the ring. The higher the value of k, the closer the ring is to the center of the image, with k=div corresponding to the region of the catheter, as shown in Fig. 2. Hence, we can limit the comparison to the vectors of the pixels belonging to a specific ring of the images (ROI). To enhance the sensitivity of correlation to the rotation of the shadows, we have also divided the image into two parts (right and left), and have calculated the average of the two correlations. The goal is to get a trend of which parts of the image change the most and assess whether this trend varies with the examination.

Figure 1. Logarithm of a RF image with div=3 and from left to right: k=3 (region of the catheter), k=2 (middle ring) and k=1 (border ring). Selecting the set (div=3,k=2), the ROI used for the correlation would be the middle ring.

In order to limit the computational time, we also define the search window as the estimated cardiac period (number of IVUS images divided by number of RF images) multiplied by the coefficient 1.3, because we assume that no cardiac period should be more than 30% longer than the estimated cardiac period. It means that after one pair RF/IVUS has been found, the correlation will be calculated only for a limited number of IVUS images (13 if the estimated cardiac period is 10 for instance). We evaluate our method of synchronization with the distribution of periods. A period is the number of IVUS frames that are unmatched between two consecutive pairs of RF-IVUS that were obtained during the synchronization. Indeed, while the virtual histology acquires an image of RF for each patient's heartbeat, the used IVUS equipment acquires at 10 frames per second. Thus, considering a rhythm of approximately one beat per second, we should get a pair RF-IVUS every 10 IVUS. Periods smaller than 7 or greater than 12 would therefore be highly unlikely, as shown in Fig. 3. To obtain an estimation of the patient average period, we simply divide the total number of IVUS by the number of RF, in each examination.
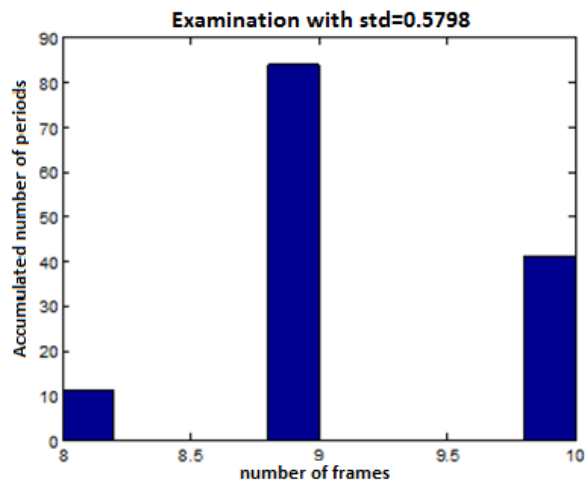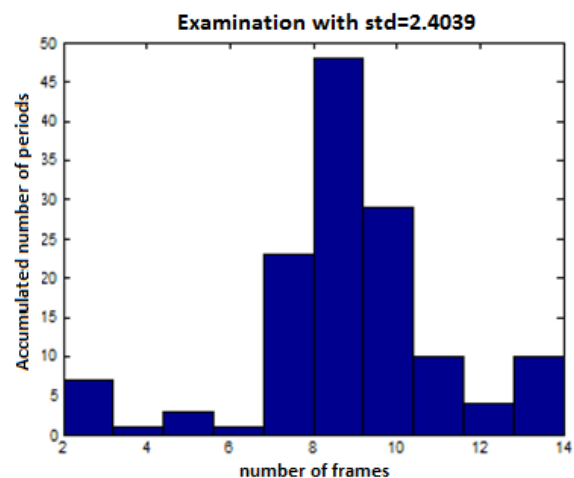
Figure 2. Unlikely histogram of the periods with standard deviation of 2.4039 (top) versus likely histogram with standard deviation of 0.5798 (bottom).

A more compact representation of those histograms is the standard deviation of the periods, which helps us automate the search of the best parameters (div and k) of the ring. Actually, the best ring corresponds to the minimum value of the standard deviation. We also verified that standard deviations below 0.65 give very good results (all the periods are very close to the mean period) and value between 0.65 and 1 are acceptable.

3.   Results

In order to evaluate the method, we propose three different approaches: one with only one set of fixed parameters, another that will find automatically the best value of standard deviation between fifteen possible sets of parameters and a last one that is equal to the second one but will stop as soon as the results are good enough. We used a laptop ASUS N73S with processor Intel® Core i7 2630QM CPU 2GHz with 8Go of RAM.

In the scenario with fixed parameters, for each of the 40 examinations, we impose the values of div=3 and k = 2, i.e., we divide the image into 3 rings and consider the middle ring as the ROI (cf. Fig. 2). 23 tests are good (standard deviation of the periods inferior to 0.65), 10 tests are acceptable (standard deviation inferior to 1). The worst result is obtained for the test 32, whose standard deviation is 1.397 (Fig. 4). We define the error rate as the number of unlikely pairs divided by the total number of RF images (which is also the total number of pairs). On the examination 32 for instance, whose patient estimated average period is 8.5 frames (1800 IVUS images for 211 RF images), we have 5 periods smaller than 6 and 9 periods larger than 10. Thus, 14 pairs out of 211 pairs are probably wrong, hence an error rate of 6.6%. Considering all exams, the obtained average error rate for this scenario was 2.8 % and average processing time was 6810 s.

In the scenario with automatic search of the best parameters set, for each examination, the algorithm now runs 15 times instead of once: each combination of parameters is analyzed, with div=3, 4, 5, 6, 7 and k = div-3, div-2, div-1. For instance, for div=3, the algorithm tests the ROI corresponding to k=2 and k=1; for div=4, the tests are done with k=1, 2 and 3, and so on. When all the values of standard deviation have been compared, the set of parameters corresponding to the smallest value is kept and the images are paired according to this optimal set. The results are much better than the algorithm with the fixed parameters div = 3 and k = 2, as shown in Fig. 4. The new average standard deviation 0.597 is significantly better than the 0.728 obtained for fixed parameters. Considering all exams, the obtained average error rate for this scenario was 1.4 % and average

processing time was 23943 s. This also proves that each study has its own peculiarities and that the algorithm should be adaptive.

Finally, in the scenario with adaptive parameters, we impose a stopping criterion in the previous algorithm to increase its speed by stopping the search of the best parameters as soon as the standard deviation is below a threshold value of 0.65. Considering all exams, the obtained average error rate for this scenario was 1.7 % and average processing time was 13984 s. The results are almost as good as those of the previous scenario (Fig. 5.) and the algorithm is twice as fast. This increase in speed is explained by the fact that the algorithm stops more often on the first values of the set of parameters: out of 40 examinations, 27 chose the pairs (div, k) = (3,1) or (div, k) =(3,2), i.e.: instead of running 15 times, the algorithm ran only 1 or 2 times for these 27 tests. Actually, the Table 1 shows that 17 examinations are equal in both scenarios, meaning that for those examinations, the third scenario saved time without worsening the results. Indeed, the standard deviation mean of 0.624 is very close to that of the second scenario 0.597. Therefore, using a stopping criterion could be a good compromise between quality of results and processing speed.
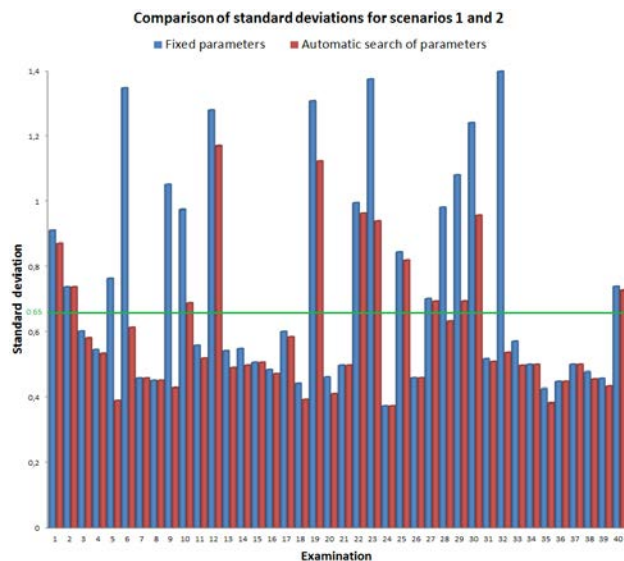

Figure 3. Comparison of cardiac period standard deviation (in number of frames) per examination for the two scenarios, with fixed parameters (div=3, k=2) and automatic search of the best parameters. Standard deviation inferior to 0.65 (green line) is considered as good.

Exam	Sc2 std	Sc2 div,k	Sc3 std	Sc3 div,k	Exam	Sc2 std	Sc2 div,k	Sc3 std	Sc3 div,k
1	0,87	5,3	0,87	5,3	11	0,52	5,2	0,56	3,2
2	0,74	3,2	0,74	3,2	12	1,17	7,5	1,17	7,5
3	0,58	7,5	0,60	3,2	13	0,49	4,1	0,54	3,2
4	0,53	4,2	0,54	3,1	14	0,50	4,2	0,63	3,1
5	0,39	6,5	0,43	4,3	15	0,51	3,2	0,55	3,1
6	0,61	7,4	0,61	7,4	16	0,47	4,3	0,49	3,1
7	0,46	3,2	0,58	3,1	17	0,58	4,3	0,60	3,2
8	0,45	3,2	0,45	3,2	18	0,39	7,4	0,44	3,2
9	0,43	7,5	0,48	5,4	19	1,12	5,3	1,21	5,3
10	0,69	3,1	0,69	3,1	20	0,41	4,3	0,46	3,2

Exam	Sc2 std	Sc2 div,k	Sc3 std	Sc3 div,k	Exam	Sc2 std	Sc2 div,k	Sc3 std	Sc3 div,k
21	0,50	3,1	0,50	5,4	31	0,51	4,3	0,54	3,1
22	0,96	4,3	0,96	4,3	32	0,54	5,2	0,54	5,2
23	0,94	3,1	0,94	3,1	33	0,50	5,4	0,57	3,2
24	0,37	3,1	0,37	3,1	34	0,50	4,3	0,52	3,1
25	0,82	5,4	0,82	5,4	35	0,38	7,4	0,41	3,1
26	0,46	3,1	0,46	3,1	36	0,45	6,3	0,45	3,2
27	0,69	4,2	0,69	4,2	37	0,50	3,2	0,50	3,1
28	0,63	3,1	0,63	3,1	38	0,45	7,4	0,58	3,1
29	0,69	5,4	0,69	5,4	39	0,43	6,5	0,47	3,1
30	0,96	5,2	0,96	5,2	40	0,73	4,3	0,73	4,3

Figure 5. Comparison of the standard deviations and chosen parameters for the scenario 2 and 3. Highlighted in gray are the examinations for which the results were equal in both scenarios.

4. Discussion and conclusion

We assessed that values of standard deviation of the periods below 0.65 correspond to a good distribution of heart beat periods, with a small range of values and allowing natural variability. Furthermore, even values close to 1, yields acceptable histogram, with a low error rate (less than 5%). The balance between speed and efficiency of the algorithm is left to the discretion of the physician who can choose between three different scenarios.

The first one applies a fixed set of parameters, here div = 3 and k = 2, which gave an error rate inferior to 6.6% in all studied cases and an average error rate of 2.8%. This set of parameters simply corresponds to a calculation of the correlation between the middle ring of the images of RF and IVUS. In the second scenario, the algorithm runs through several combinations. Here we chose a number of divisions div between 3 and 7 and k between div-3 and div-1 (div=k is the region of the catheter). The results are much improved: the average standard deviation decreases from 0.728 to 0.597 and the error rate is 1.4%. To increase the reliability of the results, the algorithm could show pairs which have unlikely periods and allow the user to accept or redo these pairs. In the third scenario, we make the algorithm stop as soon as it finds a set of parameters for which the standard deviation of the period is below 0.65. The computing time is twice smaller than for the previous scenario for roughly equivalent results.

We observed that the most significant area of the image to establish the correlation actually depends on the examination (the best histograms are obtained in different rings for each examination). To generalize the results to other acquisitions, it would be relevant to establish and assess a relationship between the standard deviation that we found acceptable (0.65) and the frequency of acquisition. This synchronization is a first step towards the reconstruction of IVUS volumes of each cardiac phase, which will allow the analysis of coronary arteries, such as the contractility throughout the phase.

Acknowledgements

References

[1] World Health Organization Department of Health Statistics and Informatics in the Information, Evidence and Research Cluster (2004). The global burden of disease 2004 update. Geneva: WHO. ISBN 9241563710.

[2] Matsumoto, Monica MitikoSoares. Análises morfológica e dinâmica da coronária baseadas no processamento tridimensional de exames de ultrassonografia intravascular . Tese de Doutorado em Cardiologia, São Paulo : Faculdade de Medicina, Universidade de São Paulo, 2010 [acesso 2012-01-15].
http://www.teses.usp.br/teses/disponiveis/5/5131/tde-25112010-143651/

[3] Matsumoto MMS, Lemos PA, Furuie SS. IVUS coronary volume alignment for distinct phases. In: Proceedings Vol. 7265. Medical Imaging 2009: Ultrasonic Imaging and Signal Processing,Stephen A. McAleavey; Jan D'hooge, Editors, 72650X

[4] Milan Sonka, Fitzpatrick JM, Handbook of Medical Imaging, volume 2. SPIE Press, Washington, USA, 2000.

[5] Monica M. S. Matsumoto, Pedro AlvesLemos, Takashi Yoneyama and Sergio ShiguemiFuruie, "Cardiac phase detection in intravascular ultrasound images", Proc. SPIE 6920, 69200D (2008); doi:10.1117/12.769670

[6] Ciompi F, Pujol O, Rodriguez-Leor O, Gatta C, Vida AS, Radeva P, Enhancing In-Vitro IVUS Data for Tissue Characterization. In Proc. IbPRIA, 2009:241-248.
http://www.teachivus.com/about.aspx

Address for correspondence
Murielle Hadad and Sergio Furuie
Laboratório de Engenharia Biomédica,
Av Prof Luciano Gualberto, Travessa 3, número 158
Prédio da Eng. Elétrica, sala D2-06 CEP 05508-010 São Paulo